ADVANCED MATERIALS
www.advmat.de

Programming Hydrogen Bonds for Reversible Elastic-Plastic Phase Transition in a Conductive Stretchable Hydrogel Actuator with Rapid Ultra-High-Density Energy Conversion and Multiple Sensory Properties

Ping Guo, Zhaoxin Zhang, Chengnan Qian, Ruofei Wang, Lin Cheng, Ye Tian, Huaping Wu, Shuze Zhu, and Aiping Liu**

Smart hydrogels have recently garnered significant attention in the fields of actuators, human-machine interaction, and soft robotics. However, when constructing large-scale actuated systems, they usually exhibit limited actuation forces (≈2 kPa) and actuation speeds. Drawing inspiration from hairspring energy conversion mechanism, an elasticity-plasticity-controllable composite hydrogel (PCTA) with robust contraction capabilities is developed. By precisely manipulating intermolecular and intramolecular hydrogen-bonding interactions, the material's elasticity and plasticity can be programmed to facilitate efficient energy storage and release. The proposed mechanism enables rapid generation of high contraction forces (900 kPa) at ultra-high working densities (0.96 MJ m^{-3}). Molecular dynamics simulations reveal that modifications in the number and nature of hydrogen bonds lead to a distinct elastic-plastic transition in hydrogels. Furthermore, the conductive PCTA hydrogel exhibits multimodal sensing capabilities including stretchable strain sensing with a wide sensing range (1–200%), fast response time (180 ms), and excellent linearity of the output signal. Moreover, it demonstrates exceptional temperature and humidity sensing capabilities with high detection accuracy. The strong actuation power and real-time sensory feedback from the composite hydrogels are expected to inspire novel flexible driving materials and intelligent sensing systems.

1. Introduction

The hydrogel actuator is a key component of soft robotic devices, which utilizes the properties of hydrogels to convert various forms of energy (temperature,[1] light,[2] voltage,[3] magnetic field,[4] pH[5]) into mechanical energy.[6] Compared with traditional rigid actuators, hydrogel actuators offer significant advantages such as reprogrammability, fast and reversible deformation.[7] To date, hydrogels have been widely deployed in soft robots, actuators, deployable devices, exoskeletons, and mechanical wound dressings.[8] However, when interfacing with large actuation systems in practical situations, hydrogels face limitations such as poor mechanical strength, slow actuation speeds, and low actuation forces (F) ranging ≈10^{-2} N or even less,[9] which poses great challenges for deploying hydrogels as actuators.

Among various hydrogels, conventional shape memory hydrogels (SMHs) exhibit multimodal stimulus response capabilities and unique programmability due to their shape memory feature, and have been widely utilized as actuators, smart switches, and artificial muscles,[10] yet they suffers from low actuation force (≈2 kPa) and slow actuation speed due to low energy density.[11] The underlying reason lies in the fact that the same permeation-based mechanism of material itself dominates the entire shape-restoring actuation.[12] For example, in osmotic actuation framework, high actuation speed necessitates the utilization of highly diffusive hydrogels, which

P. Guo, C. Qian, R. Wang, L. Cheng, A. Liu
Zhejiang Key Laboratory of Quantum State Control and Optical Field Manipulation
Department of Physics
Zhejiang Sci-Tech University
Hangzhou 310018, China
E-mail: liuaiping1979@gmail.com, liuap@zstu.edu.cn

Z. Zhang, S. Zhu
Center for X-Mechanics
Key Laboratory of Soft Machines and Smart Devices of Zhejiang Province
Department of Engineering Mechanics
Institute of Applied Mechanics
Zhejiang University
Hangzhou 310000, China
E-mail: shuzezhu@zju.edu.cn

The ORCID identification number(s) for the author(s) of this article can be found under https://doi.org/10.1002/adma.202410324

DOI: 10.1002/adma.202410324

typically carries a low modulus of elasticity, giving rise to the conflict between actuation velocity and transmitted forces.[13] Previous studies have demonstrated that altering the solvent (e.g., employing salt water as a solvent) or designing novel structures (such as asymmetric hollow hydrogel architectures) can address such conflict.[9,13] Nevertheless, the ultimate resolution lies in directly enhancing the output energy density.

To address above challenges, we report an elasticity-plasticity-controllable hydrogel material called PCTA (a composite hydrogel including polyvinyl alcohol (PVA), citric acid (CA), tannic acid (TA), and AgNPs in the reaction system, synthesis process shown in Figure S1, Supporting Information), which demonstrates a distinctive impermeable contractile mechanism akin to a hairspring inspired by energy conversion, utilizing seamless transition between elastic and plastic behavior to release large amount of energy. We utilize a suitable small molecule, CA, to program the number and properties of hydrogen bonds within the system as temperature varies. By harnessing hydrogen bond-induced changes in the elastic-plastic behavior, the hydrogel demonstrates record-high performance such as high driving force (≈900 kPa), fast deformation rate (up to 100% per minute), and an impressive output energy density up to 0.96 MJ m^{-3}. Notably, this surpasses the typical energy density of biological muscle which is ≈8 kJ m^{-3}. Molecular dynamics investigations reveal that alterations in hydrogen bond number and nature lead to distinct elastic-plastic transitions. Furthermore, our materials exhibit multimodal sensing functionality. If used as strain sensors, the engineered PCTA hydrogel stretchable sensors offer several advantages including a wide sensing range spanning from 1% to 200%, rapid response times (as low as 180 ms), and excellent linearity in output signals. If used as temperature sensors, by leveraging the high-temperature sensitivity of silver nanoparticles (AgNPs), the sensors demonstrate outstanding sensing capabilities with high detection accuracy (±1 °C) and a high temperature coefficient of resistance (TCR) of −0.043 $°C^{-1}$ within the range of 30–40 °C. Moreover, the moisture sensitivity inherent in PVA and CA components enable our hydrogels to detect changes in high-resolution humidity levels, thus broadening its sensing capabilities. Strong actuation and excellent sensing capabilities potentially enable wide applications of PCTA hydrogels in flexible smart materials.

2. Results and Discussion

2.1. Design of Energy Prestorage and Controlled Release of PCTA Hydrogel System

The hairspring is commonly used as the mechanical power source in clocks, watches, wind-up toys, and similar devices. When the hairspring is fully wound, the mechanical work (MW) is temporarily stored as elastic potential energy (EPE). One may stably hold the fully wound hairspring until movement actuation enabled by the gradual release of EPE (**Figure 1a**). This cycle of energy storage and release can be repeated indefinitely. Inspired by above concept, we have developed a PCTA composite hydrogel that excels at converting elastic deformation to plastic state for energy storage, and converting plastic state to elastic recovery for actuation (Figure 1b). The output work density and contraction strength of our developed PCTA surpass those of various elastomer actuators (Figure 1c), encompassing conventional hydrogel elastomers,[14] liquid crystal organogel elastomers,[15] polyurethane elastomers,[16] and block copolymer elastomers,[17] triggered under diverse mechanisms such as pH,[17] temperature,[14a,18] electricity,[14b,19] light,[15,20] elasticity,[21] and osmotic pressure.[14c,22]

When subjected to mechanical stretching, this hydrogel converts the MW into EPE. The key energy storage step in the PCTA is achieved by cooling, which induces a transition from an elastic state to plastic state. This process temporarily "locks" the hydrogel in its deformed shape. Upon high-temperature stimulation, the deformed shape is "unlocked," and the plastic state evolves to elastic state, resulting in the release of stored EPE which can manifest as kinetic energy (KE) or other forms of energy output.

Figure 1d illustrates a schematic representation of the hydrogen bonding state of the PCTA hydrogels at low temperatures. The introduction of CA and TA molecules into the system provides additional opportunities for hydrogen bond formation. The dynamic bonding and unbonding of hydrogen bonds can facilitate energy dissipation within the material.[23] With temperature stimulation, the hydrogen bond partially dissociates, allowing for increased mobility of the PVA molecular chain (Figure 1e). In comparison to conventional smart hydrogels which rely on volume change for actuation, our approach provides greater force and faster actuation speed by programming the elastic and plastic behavior of PCTA hydrogels through intramolecular and intermolecular hydrogen bonding transitions within the PVA network under temperature stimulation. Upon temperature stimulation, rapid dissociation of intramolecular and intermolecular hydrogen bonds occurs in PCTA, leading to its return to a highly elastic state. Consequently, stretched PCTA undergoes rapid shrinkage due to its inherent elasticity, resulting in high velocity.

2.2. Microstructure and Mechanical Properties of Hydrogels

Polymers are typically engineered to enhance their mechanical properties by designing intricate micro/nanostructures.[24] The microstructure of PCTA composite hydrogel was analyzed using scanning electron microscopy (SEM), revealing a distinct louver-like configuration (**Figure 2a**) in its flat state as fabricated (Figure 2b). When subjected to different strains, the louver blade of the PCTA composite hydrogel exhibits a partially unfolded state after energy release due to residual strain generation, indicating a strain-dependent energy-prestorage condition (Figure 2c; Figure S2, Supporting Information). This unique collapsible microstructure can be attributed to diverse interactions, including hydrogen bonds, coordination bonds, and π–π interactions between various functional groups of TA such as catechol and o-triphenyl groups with PVA molecules.[25] Meanwhile, after the introduction of the CA molecules, the PVA molecular

Y. Tian, H. Wu
Key Laboratory of Special Purpose Equipment and Advanced Processing Technology
Ministry of Education and Zhejiang Province
College of Mechanical Engineering
Zhejiang University of Technology
Hangzhou 310023, China

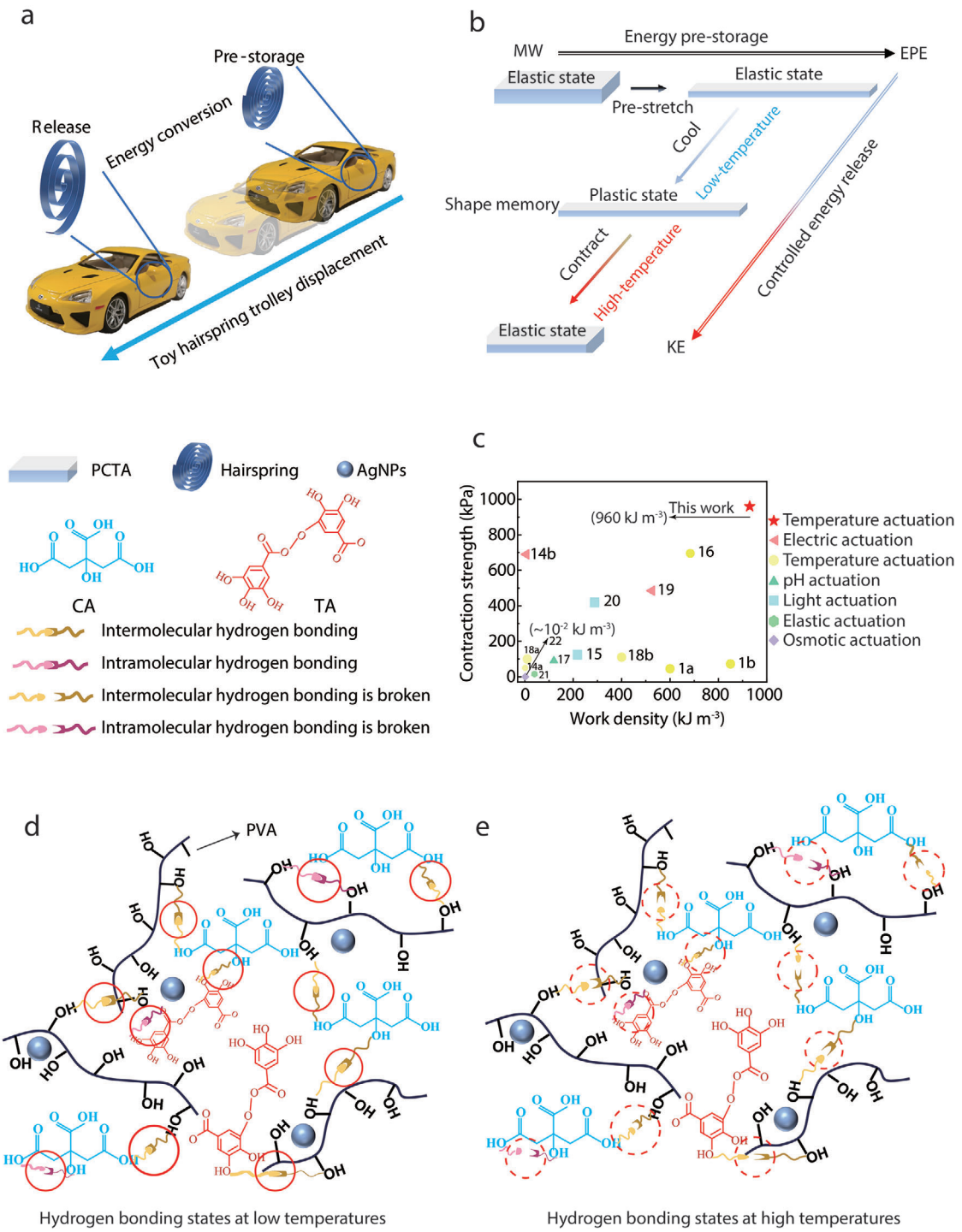

Figure 1. a) The toy car undergoes displacement through hairspring preloading and subsequent release of elastic potential energy. b) Schematic diagram illustrating the design strategy for PCTA hydrogels capable of controlled energy release by tuning the elastic-plastic phase transition under temperature stimulation. c) Our PCTA hydrogel has superior output work density and contraction strength among various synthetic contractile materials. d) Schematic representation of hydrogen bonding states at low temperatures. e) Schematic representation of hydrogen bonding states at high temperatures. Temperature stimulation programs the state of intermolecular and intramolecular hydrogen bonds.

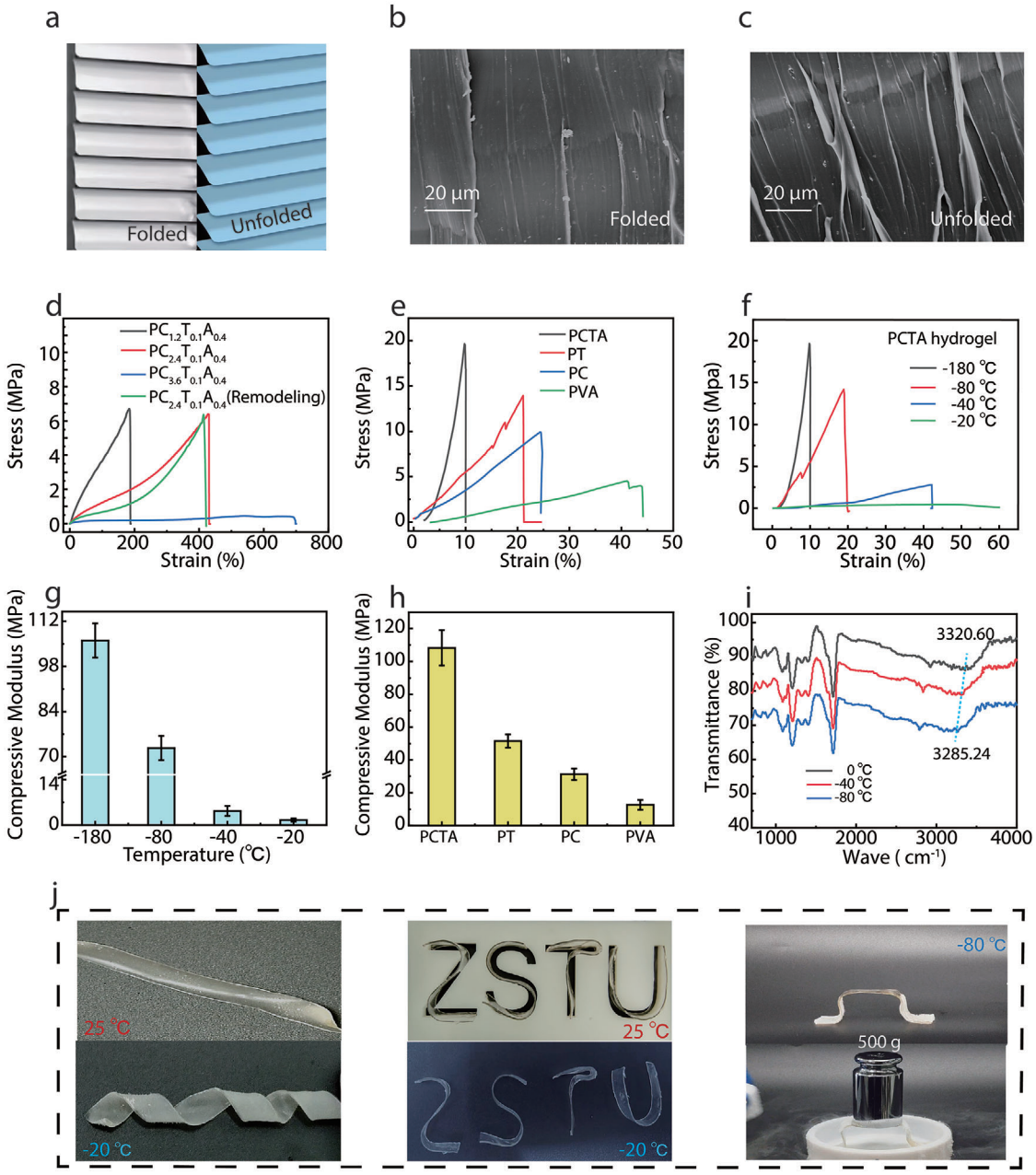

Figure 2. a) Schematic diagram of the louver. b) SEM image of the original PCTA composite hydrogel. c) SEM image of prestretched (200%) PCTA hydrogel after energy conversion. d) Tensile stress-strain curves of PCTA composite hydrogels with different component contents at 25 °C. e) Compressive stress-strain curves of PVA-based hydrogels with different compositions. f) Compressive stress-strain curves of PCTA hydrogels cooled at different temperatures. g) Young's modulus of the PCTA hydrogels with different cooled temperatures. h) Young's modulus of the hydrogels with different compositions. i) FTIR spectra of PCTA hydrogels with different cooled temperatures. j) Schematic diagram and experimental demonstration of programming PCTA hydrogels into different 3D shapes by temperature induction.

chain interacts with the hydrogen bond of the hydroxyl group of CA. As shown in Figure S3a (Supporting Information), the characteristic peak at 3252 cm^{-1} for PVA spectrum is attributed to the stretching vibration of hydroxyl group. The peaks at 2908 and 2917 cm^{-1} are related to the C—H alkyl stretching. In the PCTA spectrum, it is noteworthy that the hydroxyl group stretching peak shifts to a new wave number of 3329 cm^{-1}, indicating that PVA has formed a variety of interactions with TA and CA (mainly hydrogen bonds).[26] The X-ray diffractometer (XRD) was utilized to characterize the alteration in crystal structure of PVA following the introduction of CA molecules. As depicted in Figure S3b (Supporting Information), the original PVA exhibits a broad diffraction peak at $2\theta = 19.4°$, indicating its semi-crystalline nature. Upon addition of CA, the characteristic peak in XRD pattern for PCTA weakens, suggesting partial disruption of the original crystal structure of PVA due to molecular interactions

between CA and PVA replacing those among PVA molecules themselves.[27] Therefore, the addition of CA reduces the rigidity of crystal by modifying hydrogen bond type, leading to enhanced elasticity of PCTA at room temperature (Figure S4a, Supporting Information), thereby promoting energy release speed and driving speed under temperature stimulation. Further, the uniformly dispersed CA and TA not only provide more hydrogen bond sites for the system, but also can be used as reducing agents for in-situ generation of AgNPs. As shown in Figure S3c (Supporting Information), compared to the UV–vis spectra of PVA and PCTA composite hydrogels, a distinct absorption peak at 420 nm is observed in PCTA composite hydrogels due to the intense surface plasmonic resonance transition peak of AgNPs. Furthermore, SEM imaging of PCTA composites also reveals the presence of AgNPs (Figure S3d, Supporting Information).

Tensile tests are performed to investigate the temperature-induced conversion mechanism from elastic to plastic behavior of PCTA composite hydrogel. The resulting stress-strain curves are presented in Figure 2d and Figure S4 (Supporting Information). Notably, by adjusting the component contents, the PCTA composite hydrogel exhibits tailored mechanical properties and stretchability at room temperature. The addition of CA reduces the interaction between PVA macromolecules, thereby increasing the elongation at break.[28] Additionally, the introduction of TA results in a variety of intermolecular interactions that contribute to the mechanical properties of PCTA. The incorporation of AgNPs increases the maximum stress of PCTA efficiently; however, it results in a notable reduction in elongation at break due to the inherent rigidity imparted by AgNPs. For the $PC_{2.4}T_{0.1}A_{0.4}$ hydrogel (the mass of CA 2.4 g, TA 0.1 g, and AgNPs 0.4 g in the reaction system), an impressive break extension of 420% and a maximum stress of 6.3 MPa are achieved due to the abundance of hydroxyl groups in CA that provide numerous sites for reversible H-bond formation, facilitating maximum strain capacity and energy storage capability.[28b] The magnitude of the hysteresis loop area (U) of the PCTA hydrogel under repeated loading represents the energy dissipation capacity of the hydrogel. As shown in Figure S5a (Supporting Information), the composite hydrogel PCTA can absorb significantly more energy (e.g., 200% stretching can dissipate 0.9 MJ m^{-3} of energy), which ensures that the PCTA will not fracture during large deformation. Because of the introduction of a variety of intermolecular interactions in the system, the morphologies of the microstructure are similar to the louvered window. Such collapsible microstructure is advantageous for enhancing both the strain-sensitive characteristics and mechanical flexibility of PCTA composite hydrogel and is good for EPE storage. The loading-unloading cycles test on $PC_{2.4}T_{0.1}A_{0.4}$ hydrogel reveals small hysteresis loops and residual strains (Figure S5b, Supporting Information), demonstrating superior tensile properties and excellent resilience. The $PC_{2.4}T_{0.1}A_{0.4}$ hydrogel also exhibits easy remodeling capabilities[28b] when it was dissolved in deionized water (50 °C) to form a homogeneous solution, and then was poured into a mold to be reevaporated into a PCTA hydrogel (Figure S1, Supporting Information). The microstructure and mechanical properties do not change significantly after five remodeling cycles due to the physical cross-linking between PVA, CA, and TA molecules (Figures S1 and S6, Supporting Information).

When the prestretched PCTA composite hydrogel undergoes rapid cooling, it exhibits a remarkable transition from elastic to plastic state. The plasticity of PCTA can be evaluated through compression tests, as depicted in Figure 2e,f. After incorporating CA and TA, the $PC_{2.4}T_{0.1}A_{0.4}$ hydrogel demonstrates excellent mechanical robustness with a maximum stress reaching 20 MPa at −180 °C and a maximum compressive modulus of 106 MPa (Figure 2g,h), resembling the mechanical behavior of glassy polymers or plastics. The low water content (13.5%) and short chain slip effectively mitigate the risk of direct brittle fracture at low temperatures in PCTA.[29] To determine if there is a glass transition (commonly observed in plastics), dynamic thermomechanical analysis (DMA) was conducted on PCTA. The DMA results indicate that the loss factor ($\tan\delta$) exhibits a broad peak ≈6 °C compared to pure PVA's peak at 41.5 °C (Figure S7, Supporting Information). Take into account the molecular interactions within hydrogels, the polymer chains are constrained within a network featuring dense hydrogen bonds, hindering their motion and resulting in a "frozen chain" state similar to glassy materials.[30] This is further evidenced by the infrared spectra shown in Figure 2i, where normally, the formation of hydrogen bonds decreases the force constant of the chemical bond and leads to a shift of its vibrational frequency to a lower wave number. Specifically, the peak corresponding to hydroxyl tensile vibration demonstrates a decrease from 3320.60 to 3285.24 cm^{-1}, indicating a displacement of 35.36 cm^{-1} at that specific position. Thus, the shift in the wave number of the characteristic peak of the hydroxyl group stretching vibration of the PVA molecule with decreasing temperature attests to the enhancement of hydrogen bonding interactions.[31]

Additionally, visual evidence of the transformation from elastic-plastic behavior can be seen when the strips of PCTA hydrogel are fixed into various shapes such as bridges, spirals or letters like "ZSTU" representing Zhejiang Sci-Tech University (Figure 2j). This reversible and repetitive forming process is easily achieved by modulating the temperature repeatedly, thus demonstrating the reversibility of the temperature-induced elastic-plastic transition in PCTA composite hydrogel.

2.3. Molecular Dynamics Simulation

In our synthetic system, the presence of small molecules such as TA and CA is observed, and analysis of the stress–strain data (Figure 2d; Figure S4, Supporting Information) reveals that TA molecules primarily enhance the maximum stress exhibited by PCTA, while CA significantly influences its phase transition temperature.[32] The incorporation of CA imparts high elasticity to the material at room temperature, thereby rendering it a promising candidate for energy conversion applications. To further elucidate the mechanism underlying the temperature-induced elastic-plastic transition of PVA-based hydrogels, two molecular dynamics models, namely pure PVA model (Figure S8, Supporting Information) and composite PC model (PVA-CA composite system), are constructed. **Figure 3a** illustrates an atomistic model of composite where PVA is colored in pink and CA is colored in cyan, highlighting three types of intermolecular hydrogen bonds (labeled as PVA/PVA, CA/CA, and PVA/CA), and two types of intramolecular hydrogen bonds (labeled as

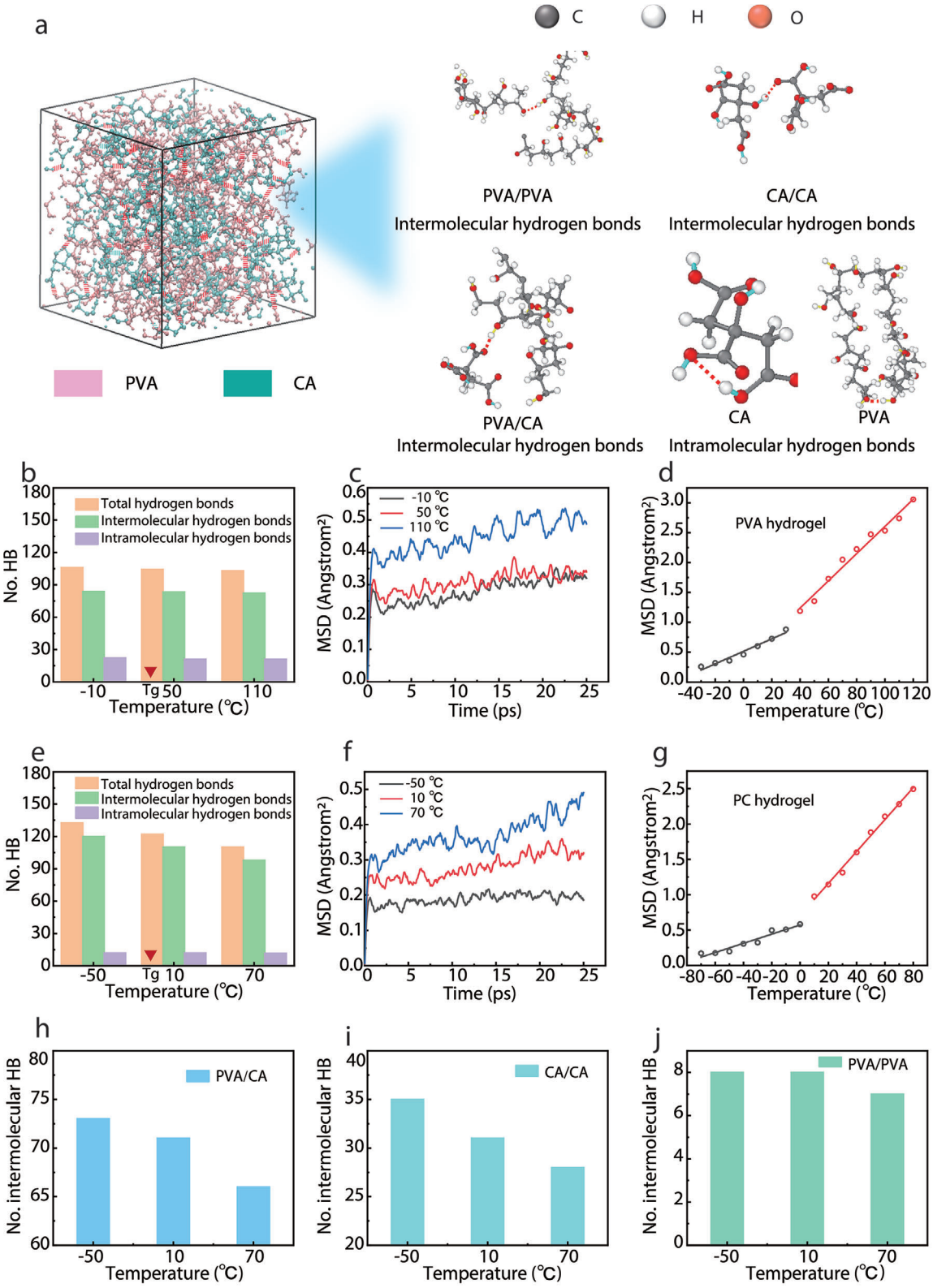

Figure 3. a) Illustration on atomistic model of PC composite hydrogel with five types of hydrogen bonds in the system. b) Number of hydrogen bonds, and c) MSD characterization in the pure PVA model at different temperatures. d) MSD characterization in the pure PVA model as a function of temperature. e) Number of hydrogen bonds, and f) MSD characterization in PC composite model at different temperatures. g) MSD characterization in the PC composite model as a function of temperature. h) The number of intermolecular hydrogen bonds of PVA/CA type, and i) the number of intermolecular hydrogen bonds of CA/CA type, and j) the number of intermolecular hydrogen bonds of PVA/PVA type, in the PC composite model at different temperatures.

CA, PVA). The introduction of CA extends the composition of hydrogen bonds from the original pure PVA model. The presence of abundant hydroxyl groups in both PVA chains and CA molecules facilitates the formation of numerous intermolecular and intramolecular hydrogen bond interactions.[33] CA is an organic acid with three carboxyl groups and one hydroxyl group. Introduction of CA into the PVA system provides additional potential sites for hydrogen bonds formation.[34] Atomistic simulations are performed using the LAMMPS[35] software package with the ReaxFF[36] force field, which is developed through first principles and includes explicit energy expressions for hydrogen bonds. VMD package[37] is used to calculate the statistics of hydrogen bonds, which are counted by geometric criteria where the donor-acceptor distance is less than 3.5 Å, and the angle between the hydrogen-donor and hydrogen-acceptor lines is less than 30°.[38] See Experimental Section for more simulations details.

A comparison between Figure 3b,e reveals an increase in the number of hydrogen bonds in the presence of CA at the temperature below, near, and above the glass transition temperatures (T_g). This suggests that enhanced interactions may result from the formation of more hydrogen bonds.[39] Prestretching and low-temperature treatment lead to greater mechanical energy storage in the hydrogel due to the presence of more hydrogen bonds. The expansion in the type of intermolecular hydrogen bonding and in the number of hydrogen bonds also explains the 420% maximum elongation at break of the PCTA hydrogel compared to the less than 50% maximum elongation at break of pure PVA. This makes PCTA hydrogel an ideal energy carrier.

Both number of hydrogen bonds in pure PVA model and in composite PC model slightly decline with increasing temperature (Figure 3b,e). However, the number of intermolecular hydrogen bonds of PVA/CA type (Figure 3h) and CA/CA type (Figure 3i) decrease a lot as temperature increases, while the number of hydrogen bonds of PVA/PVA type is rather stable (Figure 3j) and is much less sensitive to the temperature variation. In other words, temperature stimulation is highly effective for tuning the number and type of hydrogen bonds within the PCTA hydrogel, consequently leading to enhanced energy release rate and actuation speed.

Our simulation also captures the critical temperatures at which the models' transition from elasticity to plasticity occurs. We investigate the effect of temperature on the mean square displacement (MSD) of carbon atoms. As shown in Figure 3c,f, the trending of the curve (after equilibrium) reflects the self-diffusion coefficient of carbon atoms, which exhibits slower diffusion below T_g, indicating a freezing state of the molecular chain. As shown in Figure 3d,g, by monitoring the time averaged MSD over gradually increased temperature, we determine that PVA model undergoes a phase transition at 30.5 °C while the PC composite model undergoes a phase transition at 0 °C, agreeing with our previously measured DMA data (Figure S7, Supporting Information). The increased number and modified nature of hydrogen bonds within the system enable enhanced energy storage capabilities at lower temperatures and facilitate rapid energy release during heating processes, thereby enabling high actuating speeds or power.

2.4. Multiple Sensing Properties of PCTA Composite Hydrogels

The multisensory capabilities of the PCTA composite hydrogel were further investigated. The conductive pathway of the composite hydrogel is composed of in situ reduced AgNPs. As illustrated in **Figure 4a**, the relative resistance of PCTA sensors increases proportionally with applied strain. Stretching the sensor disrupts the network of AgNPs, leading to an increased tunnel distance between them and consequently resulting in higher resistance. Conversely, upon release to its initial state, the conductive path of AgNPs is reestablished, leading to decreased resistance.[40] The strain sensing performance was quantified and yielded a sensitivity factor of 2.2 (GF). Figure S9 (Supporting Information) demonstrates rapid response time (180 ms) and relaxation time (360 ms) of the sensor when subjected to a 1% stretch at a high rate of 1000 mm min^{-1}. Additionally, the electrical signals remain stable and repeatable after several stretch-release cycles at both small strains (1%) and large strains (200%) (Figure 4b; Figure S9, Supporting Information), which are sufficient for monitoring and accurately capturing real-time human movements during daily activities such as facial expression or joint flexion including knee bending or finger/wrist movement (Figure S10, Supporting Information).

Due to the thermal sensitivity of AgNPs to ambient temperature, the fabricated PCTA sensors demonstrate their utility as temperature sensors for detecting thermal stimuli. As shown in Figure 4d, the sensor's temperature coefficient of resistance (TCR) exhibits a negative correlation within the range of 30–70 °C. The decrease in conductivity with increasing temperature can be attributed to enhanced electron energization of AgNPs at higher temperatures, enabling them to overcome the energy potential barrier. When AgNPs are heated, the thermal activation of the free electrons is enhanced, thereby augmenting both their mean free path and mobility of the electrons.[41] Notably, the TCR values are −0.042, −0.012, and −0.003 $°C^{-1}$ for the ranges of 30–40, 40–50, and 50–70 °C, respectively. Furthermore, Figure 4e illustrates how the resistance values of the PCTA sensor change across a 1 °C gradient during a gradual temperature increase from 30 to 50 °C before stabilizing at a constant value when reaching equilibrium. This demonstrates that the sensor is capable of accurately detecting real-time changes in temperature. Additionally, it is worth mentioning that under varying strain conditions or temperature increasing rates (Figure S11, Supporting Information), there remains consistent resistance change in the PCTA sensor, indicating that such variation in resistance depends solely on the magnitude of temperature change. The time required for signal stabilization is directly correlated with the duration needed for the material to achieve thermal equilibrium.

The resistance of the PCTA composite hydrogel is also highly sensitive to fluctuations in humidity due to the hygroscopic nature of CA and TA, thereby endowing its advantage as a humidity sensor. The mechanism underlying the PCTA humidity sensor lies in the ability of CA and PVA to readily absorb and retain water due to their abundant hydrophilic groups. Consequently, this leads to the formation of more conductive pathways within the hydrogel, thereby enhancing its conductivity.[42] Figure 4g and Figure S12 (Supporting Information) showcase the impressive

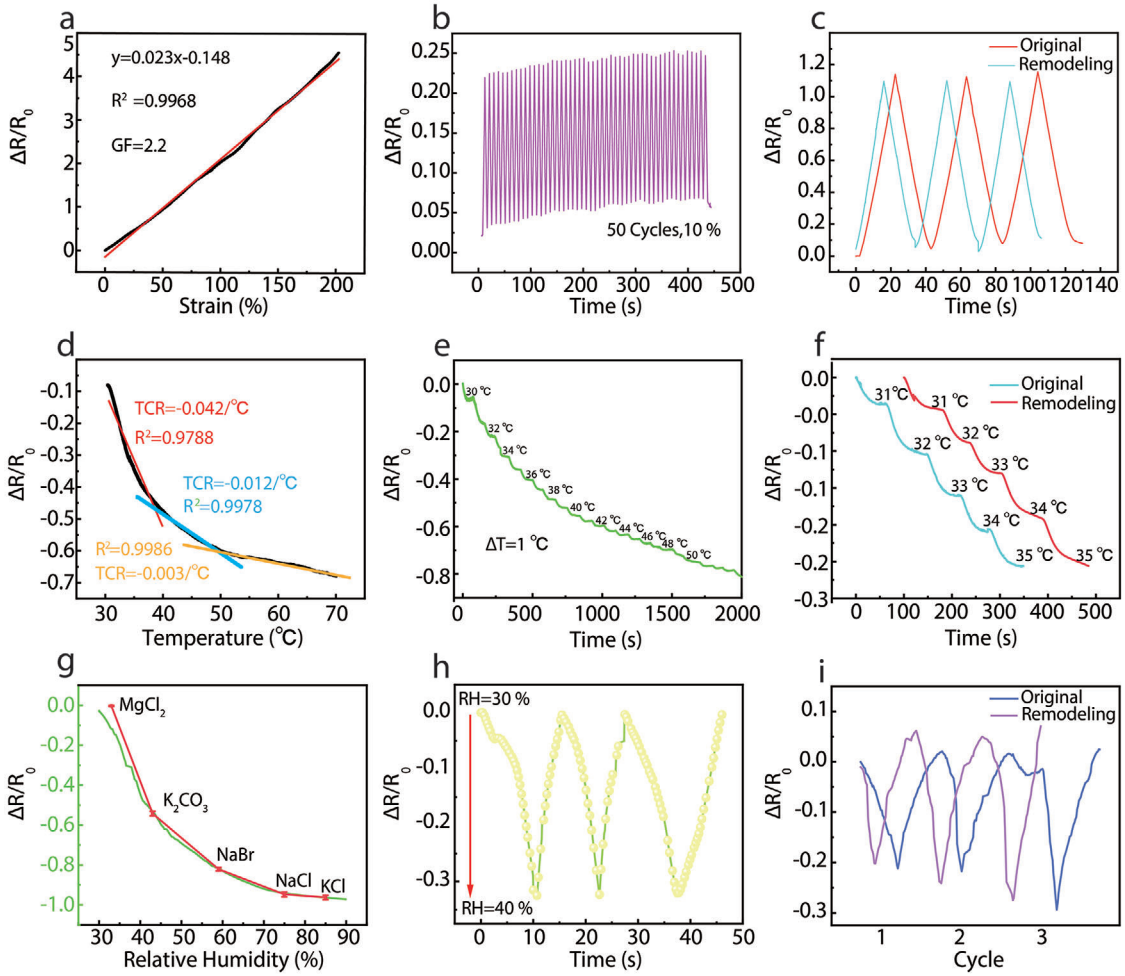

Figure 4. a) Resistance response of the sensor versus the applied strain from 0% to 200%. b) Electrical signal stability of PCTA strain sensors in 50 tensile release cycles under 10% strain. c) Strain sensing performance of the sensor before and after remodeling. d) The electrical signal varies with the increasing temperature from 30 to 70 °C. e) Relative resistance changes depending on the temperature with an increment of 1 °C from 30 to 50 °C. f) Temperature sensing performance of the sensor before and after remodeling. g) Change of relative resistance with humidity. h) Cyclic humidification-dehumidification response for three cycles. i) Humidity sensing performance of the sensor before and after remodeling.

characteristics of the PCTA humidity sensor, including a wide response range spanning from 11% to 90% humidity and an exceptional response accuracy of 5%. The accuracy of the sensing signal is finely tuned through calibration with a specific saturated solution, confirming excellent precision for this sensor. Notably, negligible hysteresis behavior is observed in the $\Delta R/R_0$ response, underscoring robust reproducibility for humidity sensing (Figure 4h). The developed sensors have been effectively utilized for monitoring facial skin moisture levels. A noteworthy aspect is that while enabling multimodal sensing capabilities, the PCTA hydrogel maintains electrical signal responses comparable to those exhibited by original materials even after remodeling (as illustrated in Figure 4c,f,i). This aspect holds particular significance from a green electronics perspective since reusable sensors have great potential for substantially reducing electronic waste generation and manufacturing costs simultaneously.[43] It is worth noting that, for multimodal sensors, the ability to distinguish signal responses from different stimuli holds significant importance. The response characteristics of PCTA to strain, temperature and humidity are different. For example, the increase in strain leads to a rise in resistance of the PCTA sensor, while the increase of temperature and humidity results in a decrease in the resistance of the PCTA sensor. Machine learning enables analysis and learning from extensive data sets to uncover patterns and relationships within the data, thereby predicting or identifying key factors influencing specific phenomena.[44] In our study, machine learning was employed to identify specific factors affecting hydrogel sensing. We established 12 groups (A-F) representing electrical signals under different strains, temperatures, and humidity conditions (Figure S13a, Supporting Information). As depicted in Figure S13b (Supporting Information), the area under the receiver operating characteristic curve (AUC) serves as a crucial measure for classifier performance evaluation. A larger AUC value indicates better classifier performance. The receiver operating characteristic curve demonstrates the validity of our model's predictions. Furthermore, we utilized a confusion matrix to assess model performance across various categories; intuitively demonstrating its capability to differentiate between

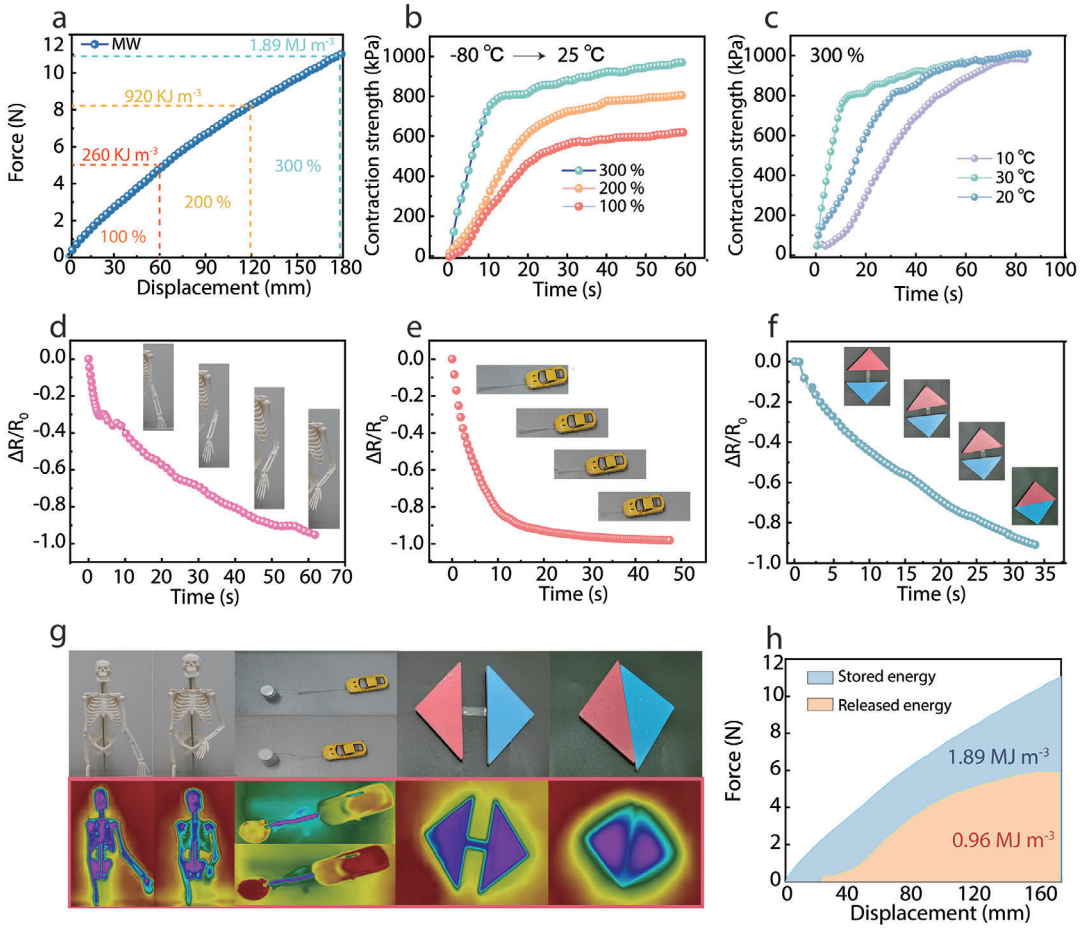

Figure 5. a) Elastic energy density as the function of prestretch ratio due to mechanical work (MW). b) Contraction strength of hydrogels with different pretensioning ratios after heating from -80° C to final temperature 25 °C. c) Contraction strength of hydrogels with different final temperatures. d) Change of relative resistance during simulated arm lifting. e) Change of relative resistance during simulated trolley movement. f) Change of relative resistance during simulated wound healing. g) Physical pictures of arm lifting, trolley moving, and wound healing and corresponding infrared imaging of these processes. h) Stored energy and released energy of hydrogel.

electrical signal changes induced by different stimuli with an accuracy rate reaching 91.7% (Figure S13c, Supporting Information).

2.5. Controllable High Energy Density Actuation of PCTA Composite Hydrogels

During the mechanical stretching of the PCTA to build up EPE, we simultaneously recording both force and length, enabling work calculation through integration of the force–displacement curve.[45] Various stretch ratios, defined in current work as the percentage of elongation over its original length (100%, 200%, and 300% in **Figure** 5a), are applied to deform the elastic PCTA hydrogel at room temperature, after which the EPE can be stored in plastic PCTA hydrogel at −80 °C. The stored EPE exhibits an expected increase from 260 to 920 kJ m^{-3}, eventually reaching a maximum of 1.89 MJ m^{-3}, for increasing stretch ratios from 100% to 300% (Figure 5a). We expect higher energy storage generates greater contraction force upon temperature simulation. The graph in Figure S14 (Supporting Information) illustrates the maximum capacity for storing elastic potential energy at various temperatures. It is observed that as the temperature decreases, there is an increase in the amount of elastic potential energy that can be stored. Additionally, this decrease in temperature enhances the actuation strength that can be achieved.

To thoroughly evaluate and understand the actuation kinetics, specifically the contraction force exerted per unit cross-sectional area, we fix both ends of PCTA samples and subsequently recording the generated forces upon temperature stimulation to room temperature (25 °C). When prepared with 300% stretch ratio, the PCTA hydrogel exhibits a contraction strength approximately equal to 900 kPa (Figure 5b). As anticipated, lower prestretching corresponds to lower contraction strengths. Moreover, PCTA hydrogels offer on-demand control over the contraction strength and energy conversion rate by manipulating ambient temperature, distinguishing them from conventional stimulus-responsive hydrogels. For instance, as illustrated in Figure 5c, the materials demonstrate varying contraction rates in response to different temperature stimuli ranging from ≈10 kPa s^{-1} up to ≈40 kPa s^{-1}, finally generating a force of 6 N. While the initial stored energy density reaches as high as 1.89 MJ m^{-3}, the

released energy density during unloading at room temperature reaches as high as 0.96 MJ m^{-3}, demonstrating a high energy conversion rate of 50.79% (Figure 5h).

The practical application of smart hydrogels necessitates careful consideration of both mechanical strength and modulus of elasticity.[46] However, conventional permeation-actuation hydrogels often face a fundamental challenge. The inherent trade-off between contraction rate and contraction force, which is influenced by factors such as elastic modulus and contraction ratio, greatly impedes their practical utility.[47] In contrast, the PCTA materials offer a promising solution to this challenge through their unique energy prestorage-controlled release actuation. In these materials, elastic contraction occurs during a rapid transition of the hydrogel from plastic state to elastic state, driven by the recoil of the PVA molecular backbone under significant tensile forces. The change in crystal state of water in PCTA hydrogels also contributes to the elastoplastic transition. Crystallization of water within PCTA at low temperatures increases overall crystallinity level. Therefore, the rigidity is further enhanced. The material becomes less deformable and is more resistant to creep and stress relaxation, which further increases energy storage capability. Upon exposure to high temperatures, ice crystals within PCTA are completely destroyed while water molecules' limiting effect on polymer chain segments disappears accordingly. This also positively affects rapid energy release behavior and actuation behavior. Importantly, this distinct actuating mechanism is not governed or limited by mass transfer. Moreover, the active recovery/actuation state of the backbone is triggered by hydrogen bonding, specifically from side groups. This feature endows the material with both high elastic modulus and high tensile properties.[21]

Beside the remarkable energy-conversion capacity, our PCTA hydrogels are also capable of multimodal sensing, opening up a myriad of possibilities across various fields, including soft robotics, biomedical engineering, and tissue engineering. These hydrogels exhibit several mechanical behaviors that not only match but even surpass those of biological muscle, underscoring their potential for revolutionary advancements. A comparison between the mechanical properties of PCTA hydrogels and mammalian skeletal muscle reveals astonishing results.[15] The stress, strain, and energy density of these hydrogels are significantly higher, exceeding those of muscle by factors of 18, 10, and 481, respectively.[18] To put this into perspective, while mammalian skeletal muscle typically exhibits stress levels of ≈0.35 MPa, strains of ≈40%, and energy densities of ≈8 kJ m^{-3},[48] the PCTA hydrogels demonstrate stress levels of 6.3 MPa with strains reaching up to 420% and energy densities as high as 3.85 MJ m^{-3}.

The unique contraction mechanism in our hydrogel can be applied in various scenarios (Figure 5g). PCTA hydrogels can be used as actuation components in the field of soft robotics or to assist wound healing in the field of cryogenic medicine. When mounted on a human skeleton model (Figure 5d; Movie S1, Supporting Information), arm movement can be achieved, realizing lifelike movement both behaviorally and structurally. Real-time detection is possible during the process of energy conversion. The sample shows remarkable contraction strength and speed, making it suitable for driving other materials into action. Figure 5e and Movie S2 (Supporting Information) show that our hydrogel can easily pull a cart while simultaneously detecting the change of electrical signal during the motion. For biomedical applications, our hydrogels could potentially serve as a smart wound dressing to promote wound healing effectively. Movie S3 (Supporting Information) and Figure 5f demonstrate the contraction and healing process using the material. The contraction rate of the hydrogel can be adjusted based on the size and depth of the wound. The effect of temperature variations on actuation performance are further demonstrated clearly via an infrared camera to record the state of motion (Movies S4, S5, and S6, Supporting Information). When PCTA is used in various practical scenarios, the stability of its system should be studied. As an ideal carrier of energy, PCTA's mechanical properties are the key to ensure the stability of energy conversion process. We recorded the process of PCTA hydrogel from prestretching to fixed shape and finally back to original length as an energy conversion (Figure S15a, Supporting Information). As shown in Figure S15b (Supporting Information), the mechanical properties of PCTA hydrogel decrease slightly after multiple energy conversion. The reason is that there is strain residual after stretching. At the same time, we also examined the repeatability of energy conversion. After five consecutive cycles of measurement, no significant attenuation of stored and released energy is found (Figure S15c, Supporting Information), which can be attributed to the favorable mechanical properties of PCTA. To further illustrate this point, we conducted an experiment involving driving a toy car using prestretched PCTA and recorded both the distance traveled and changes in electrical signals each time. As depicted in Figure S15d (Supporting Information), there is a maximum 20% variation observed in the distance covered by the car while electrical signals accurately reflect displacement changes.

3. Conclusion

Inspired by the hairspring energy conversion mechanism, in this work, we have developed a smart hydrogel with a new actuation mechanism, which modulates the intermolecular forces to change the elasticity of the material for controlled energy storage and release. Molecular dynamics simulations confirm that the changes in the number and type of hydrogen bonds lead to a unique elastic-plastic transition in hydrogels. An increase in the number of hydrogen bonds allows for more energy storage, and a change in the type of hydrogen bonds allows for faster energy release. This unique actuating mechanism and tunability of hydrogen bonding contribute to a significantly elevated actuation rate, enabling rapid energy release during the process of energy conversion. The actuation method based on energy prestorage and controllable release provides stronger and faster contraction (900 kPa, 100% min^{-1}) with better mechanical properties. In building large actuation systems, key mechanical properties (force, velocity, and modulus of elasticity) are increased simultaneously, fundamentally breaking the paradoxical relationship between the three and thus achieving a high output energy density of up to 0.96 MJ m^{-3}. In addition, PCTA have multimodal sensing capabilities with higher accuracy for strain, temperature, and humidity. Overall, the hydrogen-bonding induced rapid transition of hydrogel elastic and plastic behavior to a controlled release of energy solves the long-standing problem of weak or slow contraction of permeable hydrogels and opens the way for the rational design of powerful smart hydrogel

actuation with sensing behavior. It will expand the practical applications of smart hydrogels in artificial muscles, soft robots, flexible devices, and biomedical materials.

4. Experimental Section

Materials: Poly (vinyl alcohol) 1799 (PVA, hydrolysis:>99%) was provided by Shanghai McLean Biochemical Co., Ltd. (China). Citric acid monohydrate ($C_6H_8O_7 \cdot H_2O$, AR) and Tannic acid ($C_{76}H_{52}O_{46}$, AR) were purchased from Shanghai Aladdin Biochemical Technology Co., Ltd. (China). Silver nitrate ($AgNO_3$, ≥99.0%) was purchased from Sigma Aldrich. All other reagents are analytical-grade reagents and can be used without further purification. Deionized water (18.2 MΩ at 25 °C) from the Milli-Q Plus water purification system (Millipore) was used throughout the experiment.

Preparation of PCTA: PCTA composite hydrogels were prepared by solution casting and solvent evaporation. First, silver nitrate and CA were dissolved in 2 mL of ionized water to form a precursor solution. PVA powder (2.5 g) and TA (0.1 g) were added to 20 g of deionized water and stirred well at 90 °C until completely dissolved into a homogeneous solution. The PVA solution was cooled to 60 °C and the CA solution was added slowly. Then, $AgNO_3$ solution was added dropwise to the solution and stirred for 1.5 h. Finally, the mixed solution was poured into a round glass mold and dried in an oven for 12 h (40 °C), during which $AgNO_3$ was reduced in situ to form AgNPs. The prepared hydrogel was named $PC_xT_yA_z$, where *x*, *y*, and *z* represented the mass ratio of each component. For example, $PC_{2.4}T_{0.1}A_{0.4}$ meaned that there were 2.5 g of PVA, 2.4 g of CA, 0.1 g of TA, and 0.4 g of silver nitrate in 20 mL of precursor.

Recyclability of PCTA Flexible Hydrogels: To recover the composite hydrogel, the broken hydrogel was cut into small pieces and dissolved in water. Then ultrasonic wave was applied to the obtained mixture, similar to the steps used in preparing the original composite membrane.

Water Content Measurement of PCTA: The initial mass of the original hydrogel (m_0) was recorded, followed by subjecting it to an 80 °C oven for 48 h, and recording its finial mass (m_1). The water content was quantified using the formula $wt\% = (m_0 - m_1)/m_0 \times 100\%$.

Measurement of Contraction Strength: Mechanical test system (20 N load cell and mobile platform) was used to detect the contractile force of hydrogel (contraction strength; force per unit of cross-sectional area). The contraction force–time curve was obtained by keeping the displacement of the two fixtures of the sample at 12 mm (stretching to 200% of the original length) or 18 mm (300% of the original length) to record under temperature stimulation.

Measurement of Energy Storage and Release: Samples with original dimensions of width (a_0), thickness (b_0), and length (l_0) were recorded separately. Initially, the PCTA sample was clamped to the stretcher, and its displacement between two clamps was set at either 120 mm (stretched to 200% of the original length) or 180 mm (stretched to 300% of the original length). Subsequently, through temperature stimulation, all stored elastic potential energy within the sample was released completely and rapidly. This process resulted in high shrinkage force generation, which was recorded as a force–time curve. Next, both grippers (60 mm in original length) were restored to their initial position at a speed of 0.2 mm s^{-1} while recording the force–displacement curve during this process. By calculating contractile force per unit cross-sectional area from this curve, a contractile–time curve was obtained. The maximum elastic potential energy U_R released during contraction was determined by calculating the area under this contractile force–displacement curve. Consequently, the output working density W_E as $W_E = U_R/(a_0 b_0 l_0)$ was calculated.

Machine Learning for Signals Recognition: In this study, the multilayer Perceptron was employed to accomplish the task of discriminating between stretch, humidity, and temperature signals in hydrogel signal perception. The network architecture comprised a single fully connected layer with 10 neurons, aiming to achieve signal classification using a lightweight model while evaluating its performance through cross-validation. The rectifying linear unit (ReLU) activation function was utilized to enhance feature representation capability and improve computational efficiency.

Characterizations: The sample was frozen in liquid nitrogen for 15 min and then freeze-dried in a freeze dryer (FD-1C-50, Beijing Boyikang) at −35 °C for ≈24 h. The morphology of freeze-dried hydrogel was observed by SEM (S-4800, Hitachi, Tokyo, Japan) under 5 kV accelerating voltage. FTIR data was recorded in the wave number range of 500–4000 cm^{-1} on the infrared spectrometer (Thermo Fisher Scientific, Nicolet iS50 series). XRD curves were obtained using Cu Kα radiation (λ = 0.15418 nm) to perform 2θ scans ranging from 10° to 80° with a step size of 0.2°. The tensile test of the hydrogel at room temperature on the tensile test instrument (INSTRON, LEGEND 2366, USA) was recorded. The two ends of the rectangular sample were clamped and stretched at a certain speed of 20 mm min^{-1}. All samples tailored into the size of 30 mm × 10 mm × 0.6 mm. The sample utilized for the compression test was prepared in a cylindrical shape with a diameter of 10 mm and an approximate height of 3 mm. The compression rate employed was set at 50 mm min^{-1}. The thermal images were taken by a thermal imaging camera (Fluke Ti450Pro, America). The real-time tests of the electromechanical properties of the piezoresistive sensors were carried out by a Keithley 2400 source meter with a two-probe measurement system.

Molecular Dynamics Simulations: The PVA model consists of 12 PVA single chains, each chain containing 40 monomers. PCTA model contains 6 PVA chains and 55 CA molecules to ensure that the mass ratio of PVA to CA is close to 1:1. According to experiment results, the PVA model is equilibrated at several temperatures below T_g (−30, −10, and 10 °C), near T_g (30, 50, and 70 °C), and above T_g (90, 110, and 130 °C), and the PCTA model is equilibrated at several temperatures below T_g (−70, −50, and −30 °C), near T_g (−10, 10, and 30 °C), and above T_g (50, 70, and 90 °C). Figure 3b,c,e,f,h,i,j reports the averaged results from each group. Each simulation is equilibrated under the NPT ensemble, maintaining a constant pressure of 1 atmosphere. The time step in MD is 0.25 fs. The cutoff distance for hydrogen bond calculations in the ReaxFF force field is set to 7.0 Å. Equilibrium configurations are obtained after 500 ps of equilibration. All analyses are performed after equilibration. The number of hydrogen bonds is averaged every 25 fs for a period of 2.5 ps. The mean square displacement (MSD) trends reflect self-diffusion coefficient which is used to study the effect of various temperature on structural fluidity. The MSD of the carbon atom in Figure 3c,f are calculated every 25 fs. Figure 3d,g estimates the glass transition temperatures of two models using moving-averaged MSD of carbon atoms during a gradual heating, where uniform heating at a rate of 0.08k ps^{-1} on the PVA model at −75 °C and the PCTA model at −35 °C (Preequilibrium under the same conditions as above) are performed, respectively. The moving-averaged MSD is calculated every 10 K, corresponding to every 125 ps.

Ethical Statement: All human body-related experiments of on-skin devices on a volunteer were performed in compliance with the relevant laws and institutional guidelines, and all human subjects gave written and informed consent before participation in the experiments.

Supporting Information

Supporting Information is available from the Wiley Online Library or from the author.

Acknowledgements

P.G. and Z.Z. contributed equally to this work. This work was supported by the National Natural Science Foundation of China (No. 12272351, 23721168, 11972323, 12272337, and 12002304), and the Zhejiang Provincial Natural Science Foundation of China (No. Z24A020008, LR20A020002, and LR23A020001).

Conflict of Interest

The authors declare no conflict of interest.

Data Availability Statement

The data that support the findings of this study are available from the corresponding author upon reasonable request.

Keywords

conductive hydrogel, elastic-plastic behavior, hydrogen bonding, energy conversion, multiple sensing

Received: July 17, 2024
Revised: September 12, 2024
Published online:

[1] a) H. Liu, X. Y. Jia, R. N. Liu, K. Chen, Z. Y. Wang, T. Lyu, X. Y. Cui, Y. Zhao, Y. Tian, *J. Mater. Chem. A.* **2022**, *10*, 21874; b) S. Y. Yao, X. Y. Sun, L. N. Ye, H. Y. Liang, *Soft Matter.* **2022**, *18*, 9197.
[2] J. Deng, J. F. Li, P. N. Chen, X. Fang, X. M. Sun, Y. S. Jiang, W. Weng, B. J. Wang, H. S. Peng, *J. Am. Chem. Soc.* **2016**, *138*, 225.
[3] Y. Shin, M. Y. Choi, J. Choi, J. H. Na, S. Y. Kim, *ACS Appl. Mater. Inter.* **2021**, *13*, 15633.
[4] X. M. Du, H. Q. Cui, T. T. Xu, C. Y. Huang, Y. L. Wang, Q. L. Zhao, Y. S. Xu, X. Y. Wu, *Adv. Funct. Mater.* **2020**, *30*, 1909202.
[5] X. J. Li, Y. Cheng, J. F. Zhang, Y. R. Hou, X. J. Xu, Q. Y. Liu, *J. Mater. Chem. B.* **2022**, *10*, 120.
[6] Z. X. Huang, C. Y. Wei, L. N. Dong, A. Y. Wang, H. Y. Yao, Z. W. Guo, S. L. Mi, *Iscience.* **2022**, *25*, 104674.
[7] X. X. Le, W. Lu, J. W. Zhang, T. Chen, *Adv. Sci.* **2019**, *6*, 1801584.
[8] a) F. Y. Li, D. Y. Lyu, S. Liu, W. W. Guo, *Adv. Mater.* **2020**, *32*, 1806538; b) X. J. Cheng, L. Li, L. Yang, Q. Huang, Y. W. Li, Y. Y. Cheng, *Adv. Funct. Mater.* **2022**, *32*, 2206201; c) W. Wang, P. F. Li, R. Xie, X. J. Ju, Z. Liu, L. Y. Chu, *Adv. Mater.* **2022**, *34*, 2270321.
[9] H. Yuk, S. T. Lin, C. Ma, M. Takaffoli, N. X. Fang, X. H. Zhao, *Nat. Commun.* **2017**, *8*, 14230.
[10] a) Y. C. Zhang, J. X. Liao, T. Wang, W. X. Sun, Z. Tong, *Adv. Funct. Mater.* **2018**, *28*, 1707245; b) X. B. Hu, D. X. Zhang, S. S. Sheiko, *Adv. Mater.* **2018**, *30*, 1707461.
[11] R. C. Fei, J. T. George, J. Park, M. A. Grunlan, *Soft Matter.* **2012**, *8*, 481.
[12] a) C. Lowenberg, M. Balk, C. Wischke, M. Behl, A. Lendlein, *Acc. Chem. Res.* **2017**, *50*, 723; b) R. X. Liang, L. Wang, H. J. Yu, A. Khan, B. Ul Amin, R. U. Khan, *Eur. Polym. J.* **2019**, *114*, 380.
[13] S. Y. Zheng, Y. Y. Shen, F. B. Zhu, J. Yin, J. Qian, J. Z. Fu, Z. L. Wu, Q. Zheng, *Adv. Funct. Mater.* **2018**, *28*, 1803366.
[14] a) Y. S. Zhao, C. Y. Lo, L. C. Ruan, C. H. Pi, C. Kim, Y. Alsaid, I. Frenkel, R. Rico, T. C. Tsao, X. M. He, *Sci. Robot.* **2021**, *6*, eabd5483; b) J. K. Ko, C. Kim, D. Kim, Y. Song, S. Lee, B. Yeom, J. Huh, S. Han, D. Kang, J. S. Koh, J. Cho, *Sci. Robot.* **2022**, *7*, eabo6463; c) Y. S. Kim, M. J. Liu, Y. Ishida, Y. Ebina, M. Osada, T. Sasaki, T. Hikima, M. Takata, T. Aida, *Nat. Mater.* **2015**, *14*, 1002.
[15] Z. Jiang, B. B. Abbasi, S. Aloko, F. Mokhtari, G. M. Spinks, *Adv. Mater.* **2023**, *35*, 2210419.
[16] X. Zheng, Y. J. Chen, C. Chen, Z. Chen, Y. T. Guo, H. Li, H. Z. Liu, *J. Mater. Chem. B.* **2021**, *9*, 7371
[17] W. J. Wang, X. Xu, C. H. Zhang, H. Huang, L. P. Zhu, K. Yue, M. F. Zhu, S. G. Yang, *Adv. Sci.* **2022**, *9*, 2105764.
[18] a) R. Khodambashi, Y. Alsaid, R. Rico, H. Marvi, M. M. Peet, R. E. Fisher, S. Berman, X. M. He, D. M. Aukes, *Adv. Mater.* **2021**, *33*, 2005906; b) H. J. Sim, J. H. Noh, C. Choi, *Sensor Actuat. B-Chem.* **2023**, *378*, 133185.
[19] Y. L. Wang, J. Qiao, K. J. Wu, W. Yang, M. Ren, L. Z. Dong, Y. R. Zhou, Y. L. Wu, X. N. Wang, Z. Z. Yong, J. T. Di, Q. W. Li, *Mater. Horiz.* **2020**, *7*, 3043.
[20] Z. H. Li, Z. W. Li, S. H. Zhou, J. M. Zhang, L. Zong, *Small.* **2024**, *20*, 2311240.
[21] Y. F. Ma, M. T. Hua, S. W. Wu, Y. J. Du, X. W. Pei, X. Y. Zhu, F. Zhou, X. M. He, *Sci. Adv.* **2020**, *6*, eabd2520.
[22] a) Y. Takashima, S. Hatanaka, M. Otsubo, M. Nakahata, T. Kakuta, A. Hashidzume, H. Yamaguchi, A. Harada, *Nat. Commun.* **2012**, *3*, 1270; b) L. W. Xia, R. Xie, X. J. Ju, W. Wang, Q. M. Chen, L. Y. Chu, *Nat. Commun.* **2013**, *4*, 2226.
[23] a) H. L. Zhu, S. Z. Zhu, Z. Jia, S. Parvinian, Y. Y. Li, O. Vaaland, L. B. Hu, T. Li, *Proc. Natl. Acad. Sci. USA.* **2015**, *112*, 8971; b) X. Z. Zhang, S. Z. Zhu, *Extreme Mech. Lett.* **2024**, *66*, 102111.
[24] N. An, X. H. Wang, Y. X. Li, L. Zhang, Z. Y. Lu, J. Q. Sun, *Adv. Mater.* **2019**, *31*, 1904882.
[25] a) X. Zhang, W. F. Liu, D. T. Sun, J. H. Huang, X. Q. Qiu, Z. X. Li, X. X. Wu, *ChemSusChem.* **2020**, *13*, 4974; b) Y. N. Chen, C. Jiao, Y. X. Zhao, J. A. Zhang, H. L. Wang, *ACS Omega.* **2018**, *3*, 11788.
[26] G. Lee, M. Zarei, Q. S. Wei, Y. Zhu, S. G. Lee, *Small.* **2022**, *18*, 2203491.
[27] W. Wang, T. J. Cai, L. Tang, J. D. Zhang, C. Du, J. X. Tang, Y. Q. Yang, L. Yin, H. Kang, Z. M. Fan, *ACS Appl. Nano Mater.* **2023**, *6*, 18721.
[28] a) M. Dinari, A. Nabiyan, *Polym Composite.* **2017**, *38*, E128; b) L. R. Chen, X. H. Chang, H. Wang, J. W. Chen, Y. T. Zhu, *Nano Energy.* **2022**, *96*, 107077.
[29] Q. Ma, S. Liao, Y. Ma, Y. Chu, Y. Wang, *Adv. Mater.* **2021**, *33*, 2102096.
[30] K. Gong, L. Hou, P. Y. Wu, *Adv. Mater.* **2022**, *34*, 2201065.
[31] W. W. Niu, Y. L. Zhu, R. Wang, Z. Y. Lu, X. K. Liu, J. Q. Sun, *ACS Appl. Mater. Inter.* **2020**, *12*, 30805.
[32] K. I. Shimokawa, K. Saegusa, F. Ishii, *Colloid Surf. B.* **2009**, *74*, 56.
[33] Y. F. Cao, K. M. Zhang, H. Y. Wang, S. Y. Jiang, F. X. Lin, D. M. Guo, Y. C. Li, H. H. Huang, Z. Y. Yang, Z. G. Chi, *Chem. Eng. J.* **2023**, *476*, 146781.
[34] K. Y. Li, X. T. Yang, X. Dong, H. Y. Cao, S. J. Zhuang, X. L. Gu, *Carbohyd. Polym.* **2023**, *300*, 120258.
[35] A. P. Thompson, H. M. Aktulga, R. Berger, D. S. Bolintineanu, W. M. Brown, P. S. Crozier, P. J. I. Veld, A. Kohlmeyer, S. G. Moore, T. D. Nguyen, R. Shan, M. J. Stevens, J. Tranchida, C. Trott, S. J. Plimpton, *Comput. Phys. Commun.* **2022**, *271*,108171.
[36] K. Chenoweth, A. C. T. van Duin, W. A. Goddard, *J. Phys. Chem. A.* **2008**, *112*, 1040.
[37] W. Humphrey, A. Dalke, K. Schulten, *J. Mol. Graph.* **1996**, *14*, 33.
[38] A. Luzar, D. Chandler, *Nature.* **1996**, *379*, 55.
[39] L. J. Zhao, L. L. Wang, Y. Q. Zheng, S. F. Zhao, W. Wei, D. W. Zhang, X. Y. Fu, K. Jiang, G. Z. Shen, W. Han, *Nano Energy.* **2021**, *84*, 105921.
[40] a) C. H. Xu, Z. J. Zheng, M. Z. Lin, Q. Shen, X. H. Wang, B. F. Lin, L. H. Fu, *ACS Appl. Mater. Inter.* **2020**, *12*, 35482; b) Z. Q. Shen, Z. L. Zhang, N. B. Zhang, J. H. Li, P. W. Zhou, F. Q. Hu, Y. Rong, B. Y. Lu, G. Y. Gu, *Adv. Mater.* **2022**, *34*, 2203650.
[41] R. Yin, S. Y. Yang, Q. M. Li, S. D. Zhang, H. Liu, J. Han, C. T. Liu, C. Y. Shen, *Sci. Bull.* **2020**, *65*, 899.
[42] Z. Ahmad, M. Abbas, I. Gunawan, R. A. Shakoor, F. Ubaid, F. Touati, *Prog. Org. Coat.* **2018**, *117*, 7.
[43] X. D. Wang, Y. F. Zhang, X. J. Zhang, Z. H. Huo, X. Y. Li, M. L. Que, Z. C. Peng, H. Wang, C. F. Pan, *Adv. Mater.* **2018**, *30*, 1706738.
[44] W. Wang, H. Zhou, Z. Xu, Z. Li, L. Zhang, P. Wan, *Adv. Mater.* **2024**, *36*, 2401035.
[45] Z. W. Abdullah, Y. Dong, I. J. Davies, S. Barbhuiya, *Polym-Plast. Technol.* **2017**, *56*, 1307.
[46] a) F. Luo, T. L. Sun, T. Nakajima, T. Kurokawa, Y. Zhao, K. Sato, A. Bin Ihsan, X. F. Li, H. L. Guo, J. P. Gong, *Adv. Mater.* **2015**, *27*, 2722; b) Y. X. Dong, A. N. Ramey-Ward, K. Salaita, *Adv. Mater.* **2021**, *33*, 2006600.
[47] a) H. Sun, Y. He, Z. H. Wang, Q. L. Liang, *Adv. Funct. Mater.* **2022**, *32*, 2108489; b) C. N. Zhu, T. W. Bai, H. Wang, J. Ling, F. H. Huang, W. Hong, Q. Zheng, Z. L. Wu, *Adv. Mater.* **2021**, *33*, 2102023.
[48] T. Mirfakhrai, J. D. W. Madden, R. H. Baughman, *Mater. Today.* **2007**, *10*, 30.